Organometallic Synthesis of Magnetic Metal Nanoparticles

Marta Estrader, Aikaterini Soulantika, Bruno Chaudret

Organometallic Synthesis of Magnetic Metal Nanoparticles

Marta Estrader,*[a] Katerina Soulantica[a] and Bruno Chaudret*[a]

[a]Laboratoire de Physique et Chimie des Nano-Objets, UMR 5215 INSA, CNRS, UPS, Université de Toulouse, F-31077 Toulouse, France

*Corresponding authors: chaudret@insa-toulouse.fr, martaestrader@gmail.com

Frontispiece Image

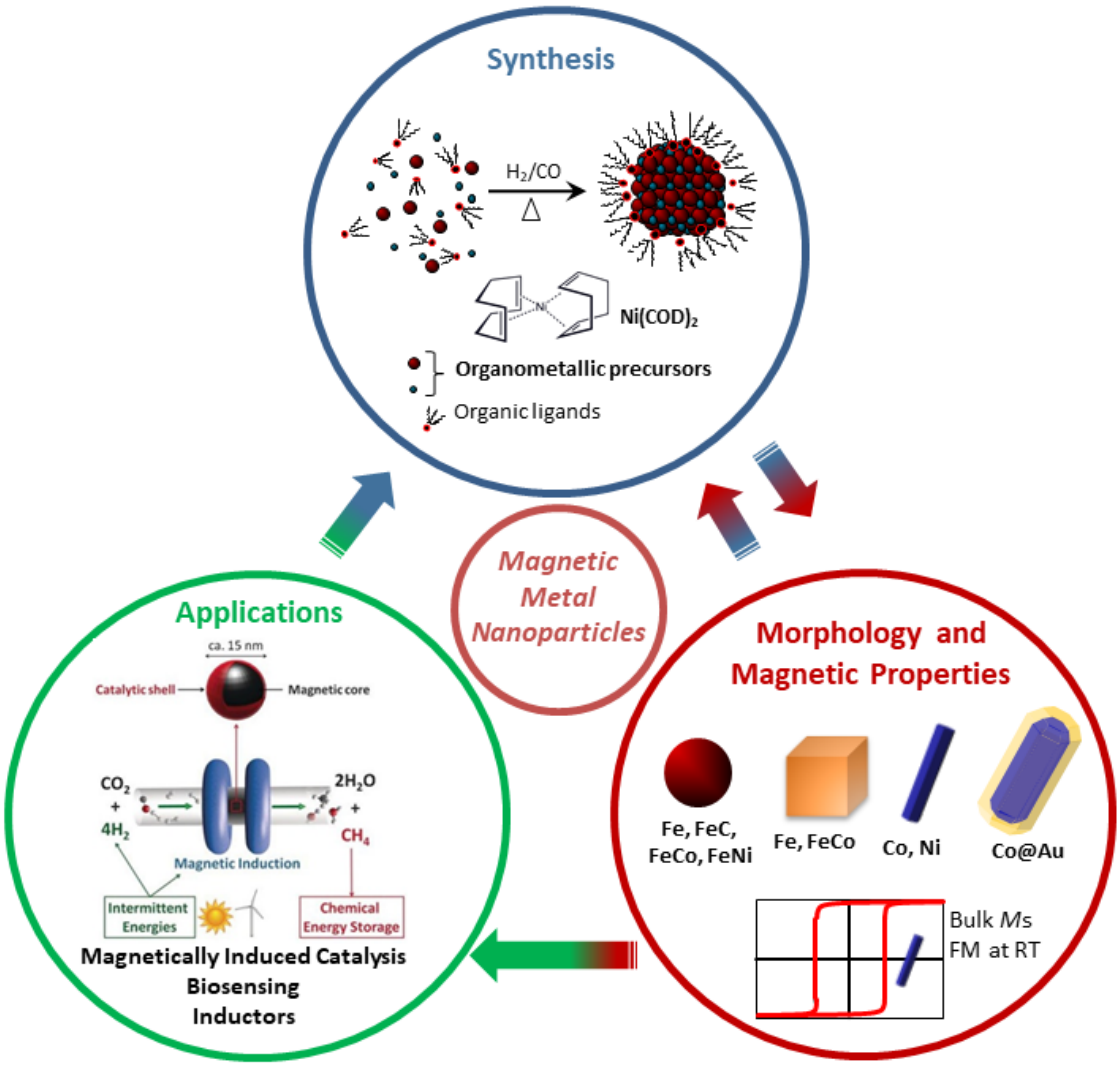

Marta Estrader is a senior Ramón y Cajal scientist in the Department of Inorganic and Organic Chemistry at the University of Barcelona (UB). She obtained her PhD from UB working on coordination chemistry and molecular magnetism (2008). She then carried postdoctoral stages in the fields of magnetic nanoparticle synthesis and nanomagnetism: ICN2 (Prof. J. Nogués; Barcelona), Stockholm University (Dr. G. Salazar-Álvarez) and LPCNO (Dr. K. Soulantica and Dr. B. Chaudret; Toulouse). Her current fields of research include synthesis of hybrid magnetic-based nanostructures, magneto/optical-structural correlations and bio/environmental applications.

Katerina Soulantica received her PhD in chemistry from the University of Athens (Greece) in 1995. From 1995 to 1998 she was a post-doctoral fellow in Spain (Prof. P. Espinet, Valladolid). In 1999, she joined the group of B. Chaudret at the LCC (Toulouse). In 2005, she joined the LPCNO laboratory as a research associate and since 2008 she is a CNRS researcher in the Nanostructures and Organometallic Chemistry (NOC) group of LPCNO. Her research domain is the synthesis of multifunctional metal nanoparticles and their applications.

Bruno Chaudret received his PhD from Imperial College in 1977. After having been Director of Laboratoire de Chimie de Coordination CNRS and Laboratoire de Physique et Chimie des Nano-Objets (LPCNO), both in Toulouse, he is presently emeritus CNRS research director and member of the French Academy of Science. His main research interests are the synthesis of nanoparticles prepared by organometallic chemistry and applications for deuterium labelling of complex molecules and for magneto-induced catalysis.

ABSTRACT

Magnetic nanoparticles (NPs) are attractive both for their fundamental properties and for their potential in a variety of applications spanning from nano-medicine and biology to micro/nano-electronics and catalysis. While these fields are dominated by the use of iron oxides, reduced metal NPs are of interest since they display high magnetization and adjustable anisotropy according to their size, shape and composition. The use of organometallic precursors allows adjusting the size, shape (sphere, cube, rod, wire, urchin, …) and composition (alloys, core-shell, composition gradient, dumbbell, …) of the resulting NPs and hence their magnetic properties. We discuss here the synthesis of magnetic metal NPs from organometallic precursors carried out in Toulouse, as well as their associated properties and their potential in applications.

1. INTRODUCTION

Magnetic Metal Nanoparticles (MMNPs) have been largely studied during the last decades as they are expected to boost the technology of a variety of applications ranging from micro-electronics and magnetic recording media, to biomedicine or catalysis.[1] Most of these applications, albeit not all, are based on the intrinsic ferromagnetism (FM) of MMNPs. Below a certain size, which depends on each metal or alloy, all the spins of a NP are aligned creating a "macrospin". These NPs are called single-domain (SD). This "macrospin" can be blocked in one direction (FM NPs) or can fluctuate to give superparamagnetic (SP) NPs. This depends upon the blocking temperature, (T_B) of the NPs which, in turn, depends upon their size and their magnetic anisotropy. These parameters are of importance for the applications, since a blocked state is required for e.g. magnetic recording applications, whereas a fluctuating macrospin will enable magnetic heating when exposed to an alternating magnetic field. For these two types of applications, hard magnetic materials such as Co or its alloys or FePt will be preferred for the former, whereas soft materials such as Fe, Ni, FeCo and FeNi will be preferred for the latter.

Historically, MMNPs in solution have been prepared by metal evaporation by resisting heating and condensation into an organic solvent at very low temperature. Upon warming the resulting solution containing the metal, the atoms condense and are transformed into clusters and NPs. G. Ozin and K. Klabunde were the precursors of this field.[2,3] However, more productive techniques needed to be developed in order to use these NPs in selected applications. Reduction methods for gold which date back to Faraday had to be adapted to produce zerovalent magnetic metal NPs. Without listing all the studies accrued out in this field, one has again to emphasize the pioneering role of K. Klabunde for the production of Co NPs upon reduction of cobalt salts with hydride or borohydride derivatives.[4] Milder reducing agents such as polyols were proved to be very efficient to produce Co NPs and nanorods (NRs).[5] Following the success in the preparation of quantum dots, similar techniques, namely high temperature decomposition of inorganic

or organometallic precursors, were also explored. This allowed, for example, the preparation of hard FePt or Co NPs.[6,7]

In this short review we focus on the synthesis of MMNPs by an organometallic approach. Besides carbonyl complexes which will not be discussed here, the decomposition of organometallic precursors is in general easy and allows a size and shape control together with a control of the surface and, importantly, the absence of surface oxidation. In the following, we will unfold efforts carried out in our group to produce MMNPs with tailored sizes, shapes and, concomitantly, magnetic properties (Scheme 1).

2. ORGANOMETALLIC APPROACH FOR THE SYNTHESIS OF MAGNETIC NPS

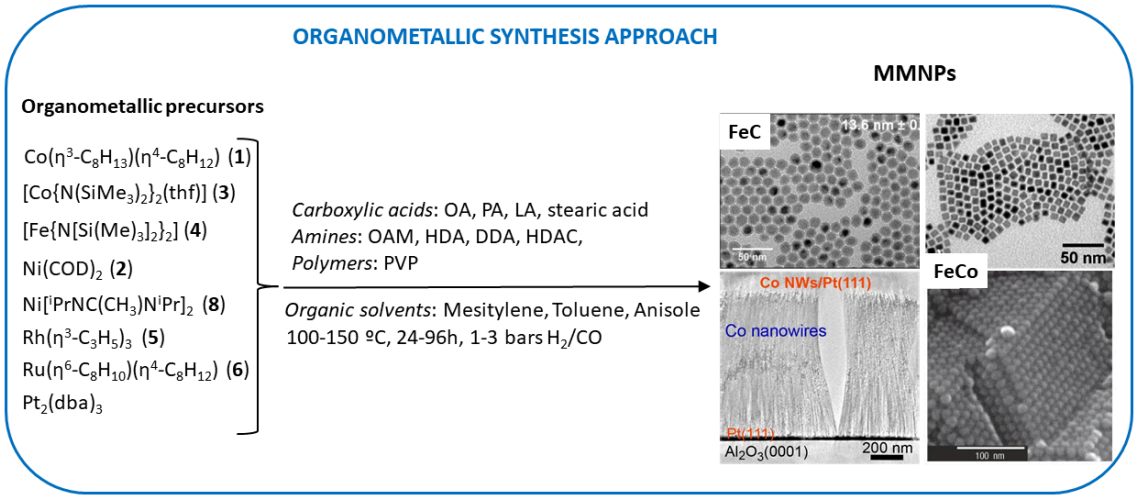

***Scheme 1*:** Overview of the main features of the organometallic synthesis approach to synthesize MMNPs.

2.1 SINGLE METAL MAGNETIC NANO-OBJECTS: Co, Fe, Ni AND FeC

Following encouraging results obtained on Ru, Pd and Pt NPs,[8] our group started in the mid-nineties the synthesis of MMNPs via decomposition of organometallic precursors in the presence of a reactive gas (H_2 or CO).[9] Importantly, the hydrogenation of olefinic ligands into the corresponding, coordinatively inert alkanes, yields NPs of non-contaminated surface, in comparison to the carbonyl route where carbonaceous species may remain on NP surfaces or even transform metal NPs into carbides.

Co NPs with mean sizes of either 1.0 or 1.6 nm can be prepared through the decomposition of Co(η^3-C_8H_{13})(η^4-C_8H_{12}) (**1**) under H_2 (3 bar) at 0, 20 or 60°C in tetrahydrofuran (THF) in the presence of polyvinylpyrrolidone (PVP).[9] In this case, only cyclooctane is produced as a by-product which does not interact with the NPs surface. The magnetic moment per atom of 1.5 nm MMNPs (μ_{Co} =1.94 ± 0.04 μ_B) is significantly

higher than the one of the bulk cobalt and similar to that observed in Ultra High Vacuum (UHV) using time-of-flight experiments for Co NPs of the same size. This constitutes a clear demonstration of the "clean" surface state of the NPs prepared under H_2 by decomposition of organometallic precursors.[10,11] It has to be noted that "clean" does not mean that the surface is naked but that the possibly interacting molecules (H_2, THF, cyclooctane,) have no effect on the magnetic moment of the NPs in contrast to oxygen, water, CO or pyridine which transform the outer cobalt layer either into an oxide or into a diamagnetic layer.

The reaction proceeds similarly with $Ni(COD)_2$ (**2**) in the presence of PVP.[12] Different sizes of Ni NPs may be obtained when changing either the chain length or the nature of the polymer used, which, in turn, influences their magnetic properties.[12–14] For instance, using PVP K 30, stable agglomerates of 30 nm composed of 3-4 nm Ni NPs were obtained which displayed a FM behaviour, whereas the use of PVP K 90 gave rise to well dispersed SP 4 nm Ni NPs.[12] Addition of coordinating ligands was shown to drastically affect the magnetic properties of the MMNPs, leading to a decrease of the *M*s in the case of π-acceptor ligands, such as CO [9,15], whereas σ-donor ligands, such as amines, were proposed to be magnetically inert.[16]

Co NPs of 2.5-3 nm could also be produced through the reaction of two different precursors, **1** and $[Co\{N(SiMe_3)_2\}_2(thf)]$ (**3**), in the presence of di-isobutyl aluminum hydride (DiBAH),.[17] NPs obtained from (**3)** had an electronically enriched shell via the coordination of amines or amido aluminum species that led to bulk magnetization whereas the use of **1** produced NPs with a decrease in magnetization, likely arising from the presence of an electron-withdrawing shell formed by alkyl aluminum species.

The next challenge was to design synthesis routes able to control size, shape, and, concomitantly, the magnetic properties of MMNPs. Larger shape-controlled Fe, Co and Ni nano-objects could be synthesized at higher temperature,[18–20] thanks to a selective coordination of the ligands on non-compact faces of the starting nuclei, a process which allows the selective growth of anisotropic NPs along a direction perpendicular to the passivated faces.[21,22]

This research started with Ni NPs of anisotropic shape obtained through hydrogenation of **2** at 70°C in the presence of hexadecylamine (HDA) or trioctylphosphineoxide (TOPO).[18] While TOPO led to a mixture of spherical NPs and tear-shaped NRs, the use of HDA led either to spherical NPs or of NRs depending on the ligand concentration. Upon using 10eq HDA with respect to Ni, 4x15 nm NRs of homogeneous size were obtained. The nature of the ligands influences not only the shape of the NPs but also their magnetic properties, since HDA stabilized NRs display a magnetization at saturation (*M*s) comparable to that of bulk Ni, whereas TOPO stabilized NPs display a reduced *M*s (0.37 μ_B per Ni atom). This result confirms that σ-donor ligands do not reduce surface magnetism in contrast to π-accepting ligands.

In the case of cobalt, hydrogenation of **1** in the presence of oleic acid (OA) produced monodisperse 5 nm NPs, whereas in the presence of long-chain amines smaller NPs were obtained.[19] However, the combination of oleic amine with OA led at 150°C to *hcp*-Co NRs of 9x40 nm, the c-axis of the *hcp* structure being the nanowire long axis. The formation of these rods was attributed to the coordination of the carboxylic acid to the lateral facets of the growing NRs. Notably, the same experiment under argon led to 4 nm NPs. By modifying the alkylamine chain length, NRs with an aspect ratio found between 1.7 and 22 were produced. All these NRs displayed a *M*s per cobalt atom very close to that of bulk cobalt, and were FM at room temperature, hence demonstrating the importance of the shape anisotropy. The replacement of OA by either lauric (LA) or stearic acid led to the formation of monodisperse NRs which assembled into 2D or 3D super-lattices (Figure 1).[23]

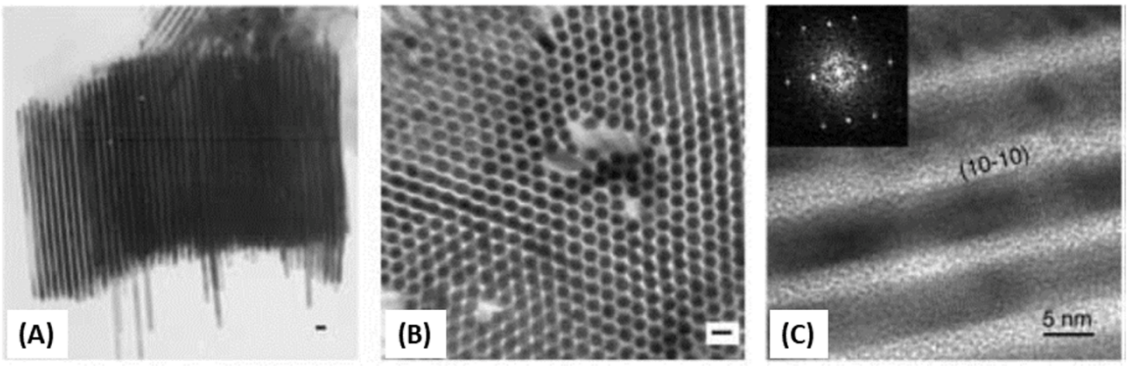

***Figure 1*:** (A) and (B) TEM images of self-organized *hcp*-Co NRs (scale bars: 10 nm). (C) High Resolution TEM (HRTEM) image and electron-diffraction pattern of some aligned rods. Reprinted with permission from Ref.[23] Copyright 2003, Wiley-VCH.

Upon changing the cobalt precursor to **3** and controlling several reaction parameters (i.e., HDA/LA ligand ratio, reaction time, addition rate of the Co precursor, etc)[24,25] Co NPs of different morphologies were selectively produced, among which, spheres, urchins and *hcp*-Co NRs of 5 nm of diameter and of a mean length controllable between 40 and 100 nm. These NRs are organized into 3D superstructures leading to very large FM superlattices displaying both a magnetization close to the bulk value and high H_C as a consequence of their large magnetocrystalline and shape anisotropies. Tandem X-ray absorption spectroscopy−small-angle X-ray scattering (XAS-SAXS) experiments have shown that 3D organization in superlattices occurs during the NRs growth in solution (Figure 2). Interestingly the NRs growth takes place first by atom-by-atom addition followed by oriented attachment.[26] Application of a magnetic field on isolated NR powders, improves the 3D organization, which is maintained after field removal. This makes these NRs good candidates for high density magnetic recording.[27]

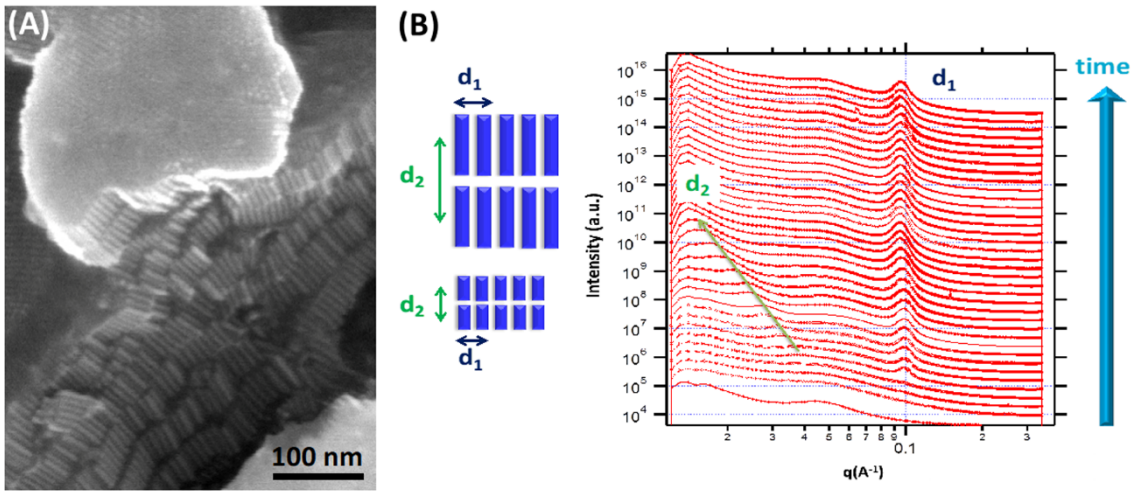

Figure 2: Ordered arrays of Co NRs. (A) Scanning Electron Microscopy (SEM) image of 3D NR superlattices composed of superimposed 2D arrays. (B) In situ SAXS time-dependent spectra of tandem for the formation of Co NRs. Reprinted and adapted with permission from Ref.[26] Copyright 2016, American Chemical Society.

The propensity of cobalt NRs to self-assemble and hence to be used for applications in which each NR could be a bit of information raised the question of the integration of these nano-objects. An original solution was to use oriented metal surfaces as 2D seeds for Co nucleation and epitaxial growth (Figure 3).[28,29] Thus Co nanowires (NWs) with their long axis perpendicular to the film plane were directly grown on non-patterned films of Pt(111), Au(111), and Co(0001) immersed in solutions containing **3** and HDA and LA. The resulting materials present an exceptional combination of high-density arrays and perpendicular magnetic anisotropy, in contrast to most arrays of FM NWs prepared by other chemical methods. Importantly, this material, when compared to isotropic NPs or patterned thin films, satisfies most of the criteria for future hard disk drives based on regular arrays of individual bits, reaching a density of up to 10 Tbits/in^2.[28] Recently, this epitaxial growth approach has been extended to the growth of Co NWs on metallic foams. The resulting material was found to be an excellent catalyst for Fischer-Tropsch Synthesis (FTS).[30]

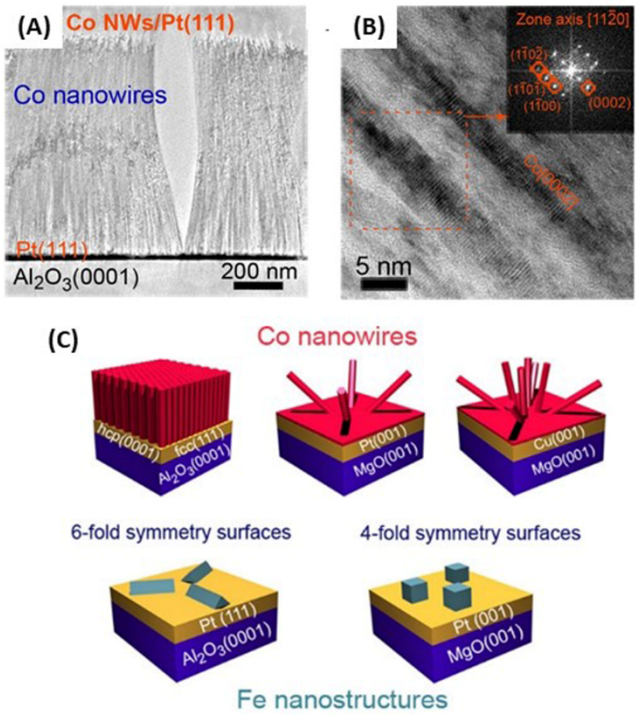

Figure 3: (A) Cross-sectional TEM micrograph of Co NW arrays grown on Pt(111)/Al_2O_3(0001). (B) HRTEM of (A). Inset: fast Fourier transforms illustrating the single-crystalline structure of the nanowires with a Co[0001] growth axis. (C) Schematic representation of Co NWs and Fe nanostructures directly grown on metallic films with different crystallographic orientations. Reprinted and adapted with permission from Ref.[29] Copyright 2015, American Chemical Society.

MMNPs, inserted into liquid crystals, can be oriented with a magnetic field, giving rise to a magneto-orientational response. The anchoring of liquid crystal molecules on the NRs can be efficient[31] due to the high surface per NR exposed, whereas the high coercive field of the NRs guarantees a large torque compared to smaller isotropic NPs. In this line, the aforementioned Co NRs (5.5x83 nm) were anchored to a polysiloxane-based polymer dissolved in toluene. The final hybrid magnetic liquid crystal polymer maintained its liquid crystalline character while preserving the magnetic properties of the NRs, hence, displaying ferromagnetism with high coercive field (6.4 kOe). Furthermore, owing to the coupling between the NRs and the polymer, the final product exhibited a more homogeneous magnetic response than similar systems dispersed in an inert organic matrix.[32,33]

This research could be extended to iron through hydrogenation of the iron analogue of **3**, $Fe\{N[Si(Me)_3]_2\}_2$ (**4**) in the presence of either long-chain carboxylic acids (OA, palmitic acid (PA)) or hexadecylamonium chloride (HDAC) and long-chain amines (dodecylamine (DDA) and HDA). In this case, the structure of iron being bcc, highly monodisperse Fe nanocubes were produced. The nanocubes arranged in close proximity and with their crystallographic axes aligned, forming extended 3D crystalline superlattices (Figure 4). The cubes were SP with *M*s (212 emu/g) very close to the bulk value (223 emu/g).[20] The discovery of room temperature magnetoresistance in networks

composed of these cubes evidenced that the organic ligands were efficient spin-conservative tunnel barriers and that these metal-organic hybrid systems were good candidates to study spin-dependent transport.[34]

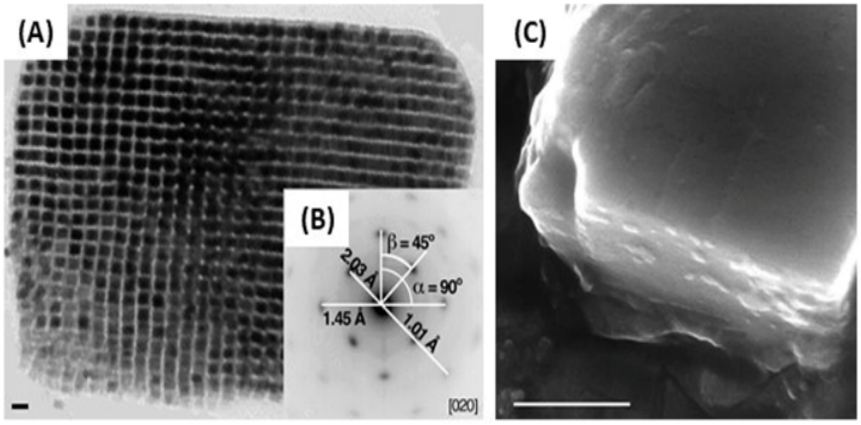

Figure 4: (A) TEM micrograph of a 3D superlattice of Fe nanocubes (scale bar: 10 nm). (B) Inset: diffraction pattern from the superlattice presented in (A). (C) SEM micrograph of a 3D superlattice (scale bar: 500 nm). Reproduced from Ref.[20] with permission from AAAS.

Similarly to Co NRs synthesis, it was found that the cubes were grown from small NPs created at the early stages of the reaction. Hence, a few years later, larger Fe nanocubes (~ 30 nm) were prepared by adapting the aforementioned synthesis to a seeded growth process (Figure 5).[35] The mechanism of their formation was thoroughly studied.[36] It was established that the nucleation and growth can occur either outside of early preformed organic superstructures composed of PA and HDA (i.e., in an isotropic environment) or inside them (i.e., in an anisotropic environment). Spherical polycrystalline NPs (1.5 to 9.4 nm) and nanocubes (side length from 13 to 27 nm) were obtained, respectively. The size control resulted from the relative concentrations of carboxylic acid and iron which controlled the nucleation and growth steps. Thus Fe(0) nuclei were formed together with a reservoir of bis(carboxylate) iron species which could only decompose onto preformed nuclei. It was later demonstrated that the cubes adopt a magnetic vortex configuration which could be stabilized, even for interacting cubes if voids are present inside them. These cubes are therefore possible building blocks for several applications, for instance magnetic recording or microelectronics.[37]

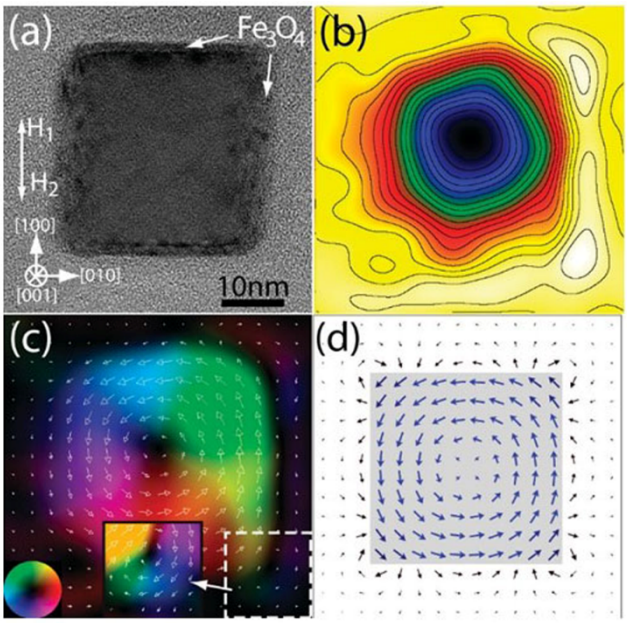

Figure 5: Electron holography and micromagnetic simulations for a single isolated Fe nanocube. (a) TEM image. (b) Phase image. (c) Vector map of the in-plane components of the magnetic induction. (d) Micromagnetic simulation Reprinted with permission from Ref.[35] Copyright 2008 American Chemical Society.

Magnetic hyperthermia is of great importance in oncology as it allows raising the temperature in tumours, thereby improving the efficiency of chemotherapy and radiotherapy through cancerous tissues damaging . The heating power of magnetic NPs in the presence of an alternating magnetic field (AMF) is quantified by the specific absorption rate (SAR, expressed in W/g), that is proportional to the specific area of the hysteresis loop (i.e., specific losses), and the excitation frequency. In this line, the magnetic hyperthermia properties of the aforementioned Fe NPs were studied as a function of their different sizes and shapes and consequently of their magnetic configuration.[38–40] It was shown that SD FM Fe NPs were optimal as they combine high M_S values and magnetic hysteresis but low magnetic anisotropy. Hence in this case, a highest SAR of 290 W/g was found for ca. 20 nm nanocubes when applying an AMF of 73 mT.[41]

The heating power exhibited by the magnetic NPs can be used as heating source to perform catalytic reactions, the NPs acting both as heating material and as catalysts (Figure 6).[42]

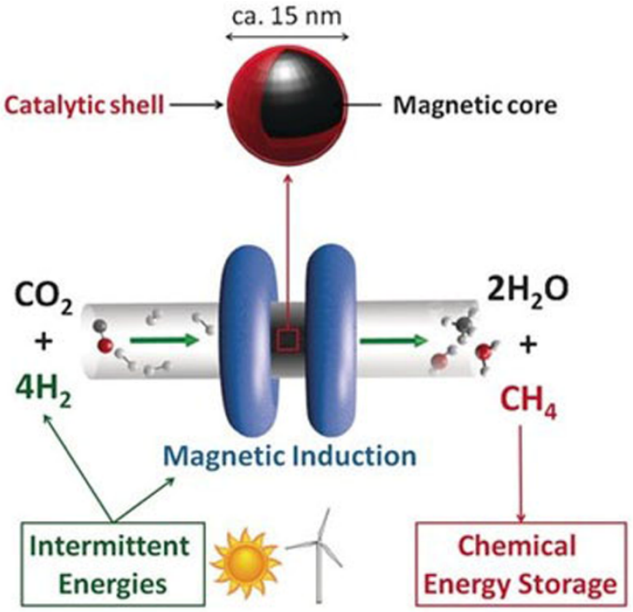

Figure 6: Schematic representation of the magnetic induced catalysis concept. Reproduced with permission from Ref.[42] Copyright 2016, Wiley-VCH.

Given the air sensitivity of Fe(0) NPs, we considered iron carbide ($Fe_{2.2}C$) as an attractive material since it combines a much better air-stability and a high magnetization, thus exhibiting higher SAR values at lower AMFs, and is an active catalyst for the Fischer-Tropsch synthesis. $Fe_{2.2}C$ NPs were synthesized from preformed Fe NPs through two chemical routes[36]: i) addition of $Fe(CO)_5$ to Fe NPs, since the carbonyl precursor can provide both Fe and carbon (Figure 7)[43] and ii) carbidization of Fe NPs by exposure to a mixture of CO and H_2 (syngas), which is known to transform iron into iron carbide during the Fischer-Tropsch process (Figure 8).[42] Importantly, the two approaches, allowed tuning the final composition of the iron carbide and thus, its SAR, reaching values up to 2100 W/g using only 47 mT at 93 kHz.

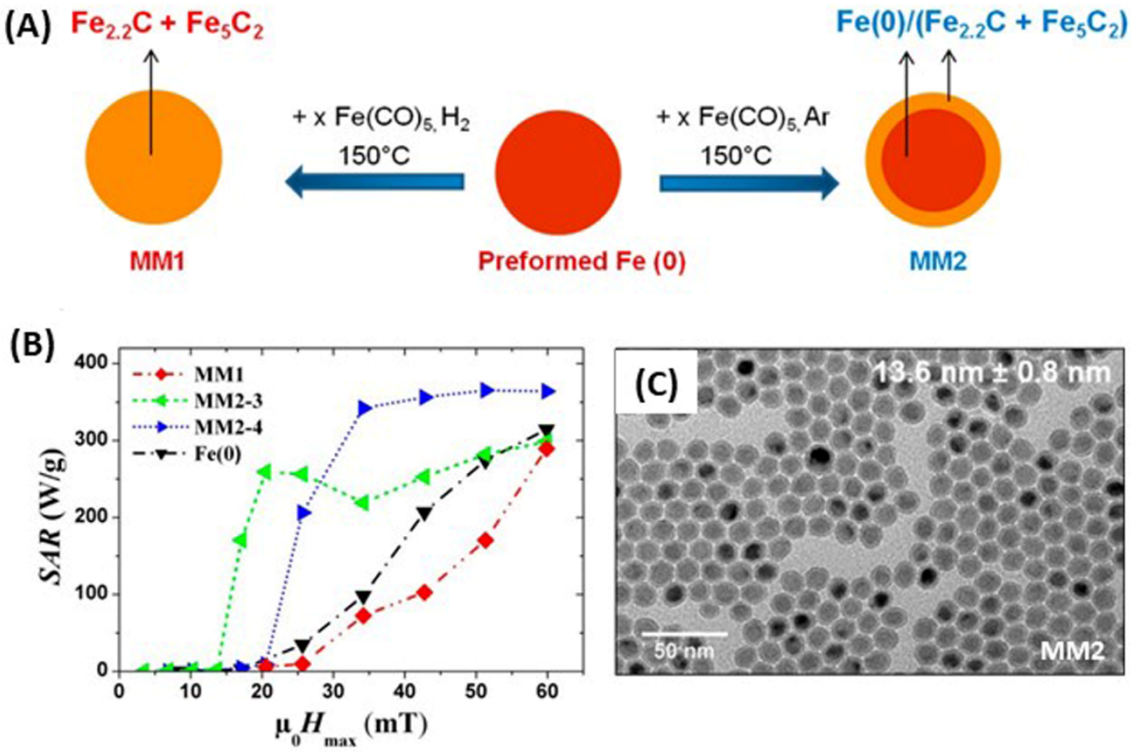

Figure 7: (A) Synthesis of iron carbide (MM1) and iron(0)/iron carbides core@shell (MM2) NPs from preformed iron(0) NPs. (B) SAR measurements. (C) TEM image of MM2 NPs. Reprinted and adapted with permission from Ref.[43] Copyright 2012 American Chemical Society.

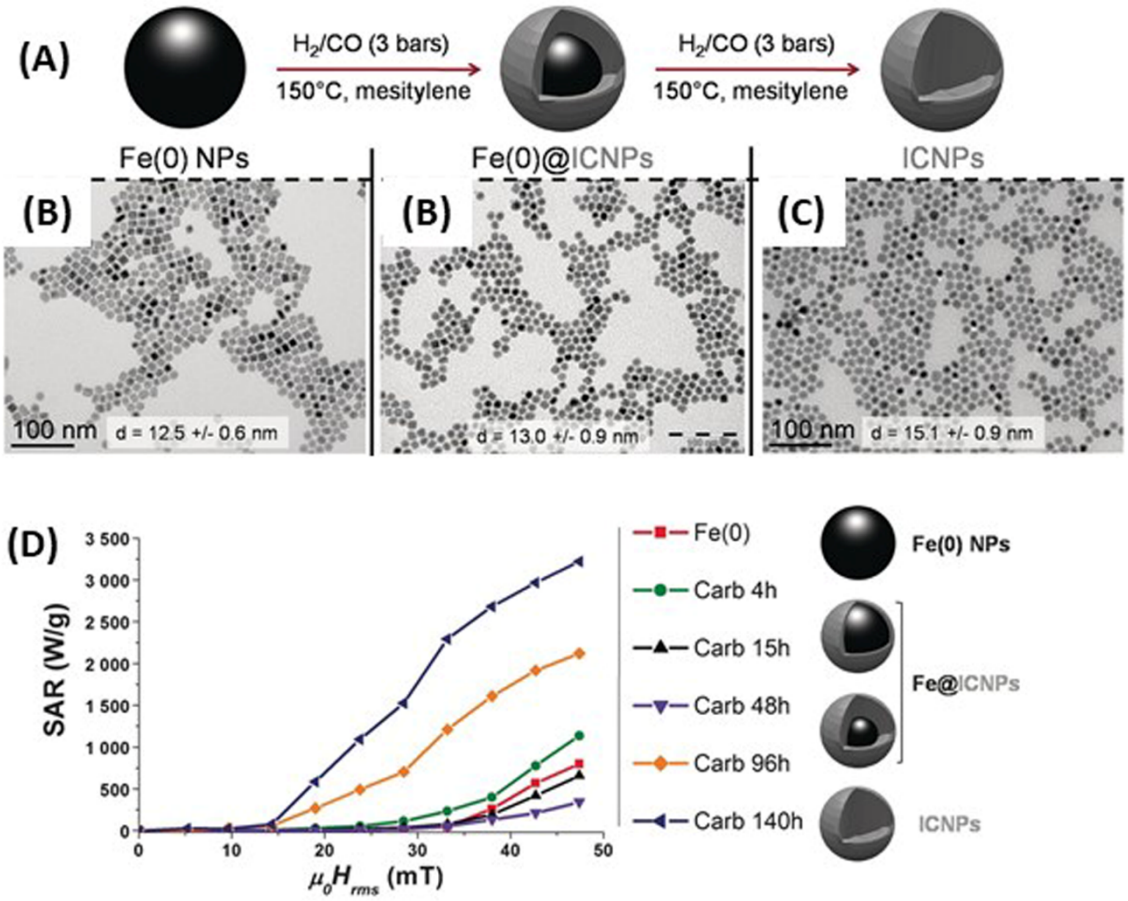

Figure 8: (A) Carbidization procedure. TEM images of (B) starting Fe0 NPs, (C) after 15 h carbidization and (D) after 140 h carbidization (scale bar: 100 nm). Reprinted and adapted with permission from Ref.[42] Copyright 2016, Wiley-VCH.

Recently, the carbidization reaction has been optimized by controlling the concentration of the ligands at the beginning of the reaction. In addition, the origin of the heating properties of $Fe_{2.2}C$ NPs has been addressed in detail. It has been found that a minimum quantity of surface ligands is required to allow the NPs to align into chains when applying a magnetic field, which provides an uniaxial anisotropy responsible for the heating power enhancement.[44] Hybrid platforms composed of $Fe_{2.2}C$ NPs supported onto SiRAlOx, impregnated by small NPs, either Ru or Ni, are excellent catalysts for the CO_2 hydrogenation reaction.[42] Furthermore, the $Fe_{2.2}C$/Ni/ SiRAlOx system has been mixed with magnetically hard *hcp*-Co NRs.[45] In this combination, by application of a low intensity field the *soft* magnetic material ($Fe_{2.2}C$) allows the system to reach the temperature necessary to trigger the heating action of the *hard* magnetic material (*hcp*-Co). Since Co exhibits FM behavior until roughly 1000 °C, this combined platform is a promising catalyst for high temperature catalytic reactions such as methane reforming.

2.2 ORGANOMETALLIC SYNTHESIS OF BIMETALLIC NANO-OBJECTS

The organometallic approach is fully adapted to produce bimetallic nano-objects. By playing on the nature of the precursors and the reaction conditions, and depending on the desired properties, alloys, core-shell structures or hetero-structures could be prepared. Of special importance is the relative rate of decomposition of the two precursors which can orientate the synthesis towards alloys or core-shell NPs, whereas successive decomposition of different precursors can lead to core-shell NPs or hetero-structures. Thus, it was possible to prepare in this way: i) hard magnetic materials with possible applications in data storage, MEMS/NEMS, etc (CoRh, CoPt, FeRh); ii) soft magnetic materials for applications in micro-electronics or magnetically induced catalysis (FeCo, $FeNi_3$, Fe@Ru, Fe2.2C@Ru, …) and iii) hetero-structures such as magneto-optical systems for biosensing applications (Co-Au, Co@SnPtAu).

Small (1-2 nm) SP CoRh, CoRu and CoPt NPs were obtained by hydrogenation at room temperature in solution of a mixture of **1** and the organometallic precursors $Rh(\eta^3\text{-}C_3H_5)_3$ (**5**), $Ru(\eta^6\text{-}C_8H_{10})(\eta^4\text{-}C_8H_{12})$ (**6**) and $Pt_2(dba)_3$ (dba= bis(dibenzylideneacetone)), respectively in the presence of PVP,[14,46–49] as for Co NPs.[9] Whereas the presence of Rh enhances the coercivity of Co NPs, the presence of Ru leads to soft magnetic NPs.[47,48] Similarly, 2 nm FeRh NPs of different compositions ($Rh_{20}Fe_{80}$ and $Rh_{50}Fe_{50}$) were synthesized by simultaneous decomposition of stoichiometric quantities of **4** and **5** but using two different routes for the reduction process: the standard hydrogenation procedure or an amino-borane reducing agent.[50–52] Interestingly, reaction of the mixture of the two precursors with hydrogen produces Rh@Fe NPs whereas the use of aminoborane leads to Fe@Rh NPs.[53] This demonstrates the fine tuning organometallic chemistry can bring to materials synthesis. All NPs are SP, showing magnetic polarization at the Rh atoms.

The FeCo alloy ($Fe_{50}Co_{50}$) exhibits the highest Ms value (bulk = 235 emu/g) along with a low anisotropy constant ($1.5 \times 104\ J{\cdot}m^{-3}$) and a Curie Temperature above 1000°C which confers to this material the required properties for boosting the performances of inductors in microelectronic applications as well as performing high temperature reactions. FeCo nanocrystals of ca. 15 nm mean size and adopting the stoichiometry $Fe_{0.61}Co_{0.39}$ or $Fe_{0.58}Co_{0.42}$ were synthesized by using the precursors $Fe(CO)_5$ (**7**) and **1** as well as **7** and (**3**) respectively.[54,55] The Ms of all NPs prepared in this way was rather low (160 emu/g) which was attributed to the formation of amorphous carbides resulting from the presence of CO in **7**. Interestingly, the 15 nm spherical FeCo NPs are arranged into 3D super-lattices reaching multi-millimeter sizes and the magnetic measurements showed an increase of *Ms* from 160 to 183 emu/g for the sample when **3** was used (Figure 9). The internal structure of FeCo NPs was found to lack long-range atomic order, showing an onion-like composition consisting of a Co core surrounded by an Fe shell, hence accounting for the low Ms of the NPs as compared to the bulk value. Annealing these FeCo NPs leads to an increase of the *Ms*, which was attributed to a disordered-ordered phase transition and the excretion of carbon. Importantly, due to the presence of dipolar interactions, the millimetre supercrystals adopted an antiferromagnetic

configuration which complies with the requirements for a high permeability in the gigahertz range that could be applied in low-consumption microelectronic devices.[54]

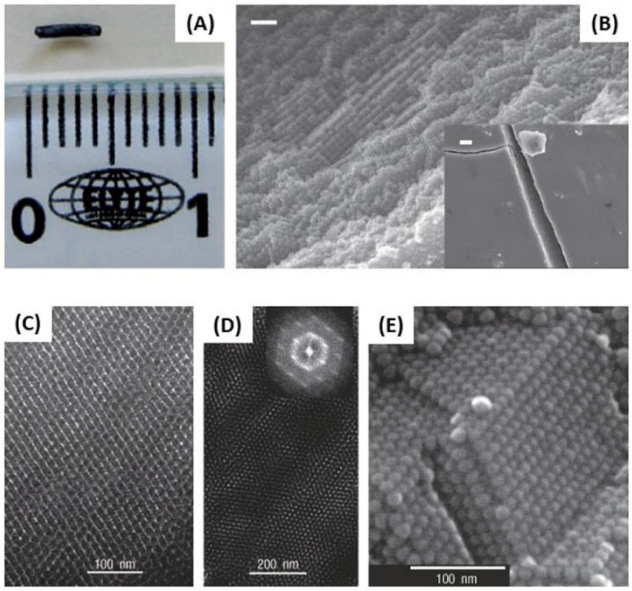

Figure 9: Global views of FeCo supercrystals from a macroscopic to a nanometric scale. (A) Photograph of one 4-mm-long supercrystal. (B) SEM micrographs of a supercrystal (scale bar: 10 nm; inset scale bar: 1 µm). (C) and (D) TEM micrographs after ultramicrotomy a supercrystal(inset in D: Fourier transform of the image). (E) SEM micrograph of a broken supercrystal. Image reprinted with permission from Ref.[54] Copyright 2005, Springer Nature.

In 2019, a new synthesis protocol for the production of FeCo NPs has avoided the formation of carbides by using only Fe and Co amide precursors (**4** and **3**).[56] Depending on the ligands employed, different sizes and internal structures were produced. Thus, when using PA and HDA, 8 nm FeCo NPs were obtained,, characterized by a gradient of the relative concentration of both metals across the NP, the shell being Fe-rich. In contrast, upon replacing PA by HDAC, FeCo NPs of 11 nm were obtained. For these NPs, a short-range ordered B2 FeCo phase (CsCl structure) was observed (Figure 10). This was the first time that this order was directly formed through a liquid-phase synthesis. Interestingly the presence of this phase could be assessed by using zero field Co nuclear magnetic resonance. Furthermore, these *bcc* B2 FeCo NPs exhibited magnetic properties very close to those of bulk cobalt (Ms = 226 emu/g). After mixing them with epoxy monomers, they could be integrated on inductor-based filters, leading to a 27% enhancement of the inductance value at 100 MHz.

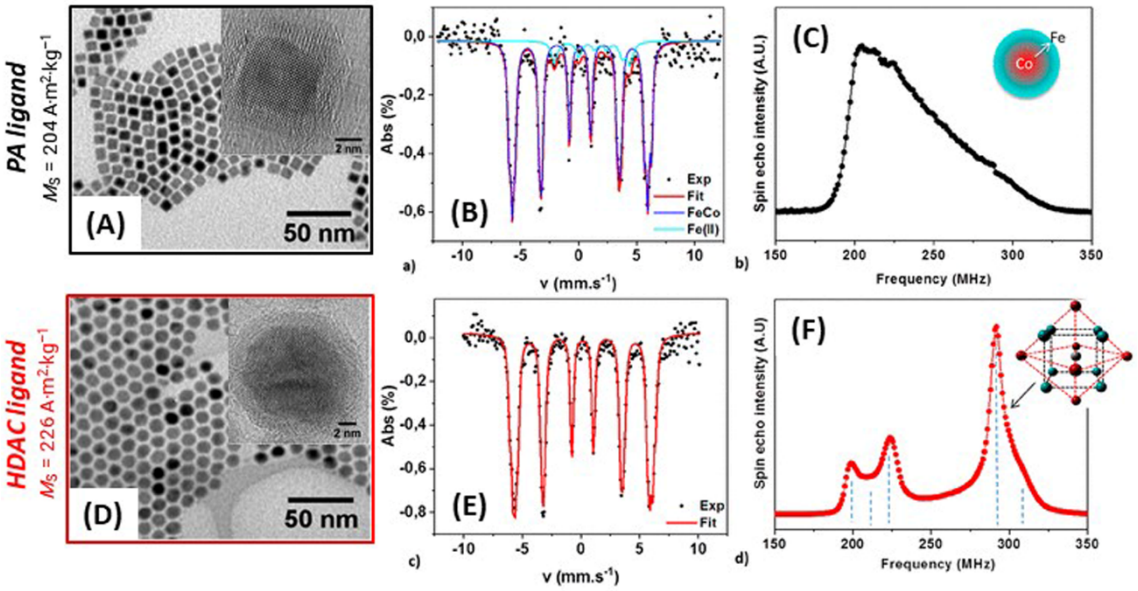

Figure 10: (A) and (D) TEM images of FeCo NPs prepared with PA (FeCo-PA) and HDAC (FeCo-HDAC), respectively. Insets: HRTEM images of a NP from (A) and (D). (B, E) 5 K 57Fe Mossbauer spectrum and (C, F) ^{59}Co FNR spectrum of the (B, C) FeCo-PA and (E, F) FeCo-HDAC NPs. Inset: schematic view of the gradient profile determined for PA NPs and B2 order for the HDAC NPs (Fe, blue; Co, red). Reprinted and adapted with permission from Ref.[56] Copyright 2019, American Chemical Society.

In another approach, preformed Fe NPs were also used as seeds to form Fe@FeCo core@shell NPs, after reaction with $Co_2(CO)_8$.[57] The Fe@FeCo NPs of roughly 12 nm, exhibited *Ms* values (206 emu/g) similar to the starting Fe NPs seeds (198 emu/g), thus, quite close to Fe bulk values. Importantly, this system under an alternating magnetic field exhibited SAR values of 284 W/g in solution. This heating power was used to prove the concept of magnetically induced catalysis in the CO hydrogenation reaction.

Similarly, the FeCo NPs prepared from **3** and **4** were used for different catalytic reactions occurring at temperatures between 300 and 700°C, which could be addressed thanks to their high Curie temperature.[58] However, at these reaction temperatures, namely propane dry reforming (ca 500°C), methane dry reforming (ca 600°C) and propane dehydrogenation (ca 700°C) an extensive sintering of the catalytic NPs was observed. In order to circumvent this problem, the NPs were embedded into a carbon layer and Ni NPs were deposited on the surface of the carbon.[59] This led to excellent results for dry reforming reactions in terms of conversion and selectivity thanks to the limitation or complete suppression of sintering. This system even enabled dehydrogenation of propane, hence demonstrating the high temperature reached by the NPs.

The synthesis of FeNi NPs was also studied in search of soft magnetic nanoalloys for their use in various magnetism-based applications (inductors, magnetic shielding, magnetic refrigeration and magnetically induced catalysis). The first attempt to produce

FeNi NPs led to small sizes (2.8 nm) when hydrogenating **2** and **4** in the presence of stearic acid and HDA.[60] The NPs featured a gradient composition where the iron-rich shell did not allow obtaining the desired soft magnetic material. Searching for larger FeNi NPs with controlled composition, the recent method reported to produce FeCo NPs was adapted.[56] $Fe_{30}Ni_{70}$ NPs were synthesized by co-decomposition of **4** and $Ni[^iPrNC(CH_3)N^iPr]_2$ (**8**) under H_2 and using PA. By varying the Ni/Fe ratio, the reaction temperature and the time, a range of sizes (14.4 to 22.3 nm) and SAR values from 200 to 820 W/g were attained (Figure 11A).[61] Since Ni is a catalyst of choice for many reactions, these FeNi NPs were tested both as heating agent and as catalyst for the CO_2 hydrogenation reaction. The low CH_4 selectivity observed was attributed to a Fe-rich shell. This drawback was overcome by enriching the NP surface in nickel through additional decomposition of **4** under H_2 onto preformed $FeNi_3$ NPs (Figure 11B). Importantly, $Fe_{30}Ni_{70}$@Ni NPs displayed excellent heating power and catalytic activity (100% CO_2 conversion and 100% CH_4 selectivity).

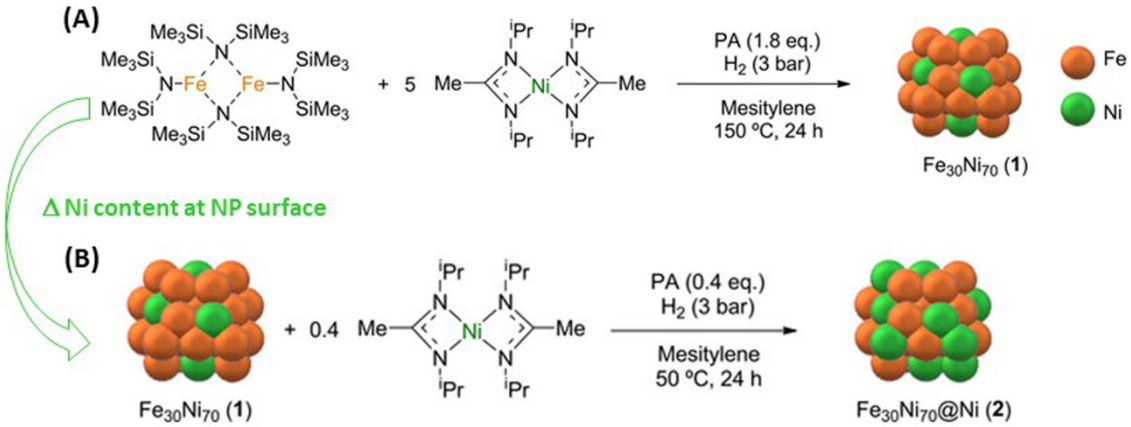

Figure 11: (A) and (B) Schematic representation of the synthesis procedure of $Fe_{30}Ni_{70}$ and $Fe_{30}Ni_{70}$@Ni NPs, respectively. Reprinted and adapted with permission from Ref.[61] Copyright 2016, Wiley-VCH.

Water electrolysis is the process of choice for the production of green hydrogen but generally uses high-cost noble-metal-based electrocatalysts. A noble-metal-free catalyst, namely $Fe_{2.2}C$@Ni, has been recently developed through the organometallic approach. It takes advantage of its magnetic heating properties to improve the oxygen and hydrogen evolution processes of the water electrolysis reaction, hence demonstrating the interest of magnetic activation.[62] The $Fe_{2.2}C$@Ni NPs were obtained by depositing a Ni shell through the decomposition of $Ni(acac)_2$ on the surface of preformed $Fe_{2.2}C$ NPs[42] in the presence of PA.

Fe@Ru[57] and $Fe_{2.2}C$@Ru[63] core@shell NPs of mean sizes between 10 and 20 nm were designed to fulfil the two requirements needed for having a single object displaying both heating and high catalytic properties. In this respect, a discontinuous shell of Ru was deposited onto preformed Fe and $Fe_{2.2}C$ NPs by decomposition of $Ru_3(CO)_{12}$ or **6** in the presence of H_2. The presence of Ru on the surface led to a decrease of *M*s (170 and 160

emu/g for Fe@Ru and $Fe_{2.2}C$@Ru, respectively).[63] In these NPs, the discontinuous Ru shell was grown through two decomposition steps of the $Ru_3(CO)_{12}$ precursor (Figure 12A). These systems were used to carry out reactions in solution. It was demonstrated that the surface of the NPs can be heated in solution well above the boiling point of the solvent, e.g. at 236°C, in toluene, the mean temperature of which remains 110°C. This overheating of the NP surface allows to carry out difficult reactions such as the hydrodeoxygenation (HDO) of aromatic and aliphatic ketones, a reaction that in conventional thermal catalysis requires very high temperatures and pressures. Thus, using $Fe_{2.2}C$@Ru NPs in mesitylene under 3 bars H_2, the complete conversion of acetophenone into ethylbenzene[64] and of biomass platform molecules, such as hydroxymethylfurfural into dimethyl furane, was observed[63] (Figure 12B).

The same approach was employed with FeNi@Ni NPs. They display a higher activity in HDO, but also allow the hydrogenolysis of diaryl ethers which are models of lignin constituents.[65]

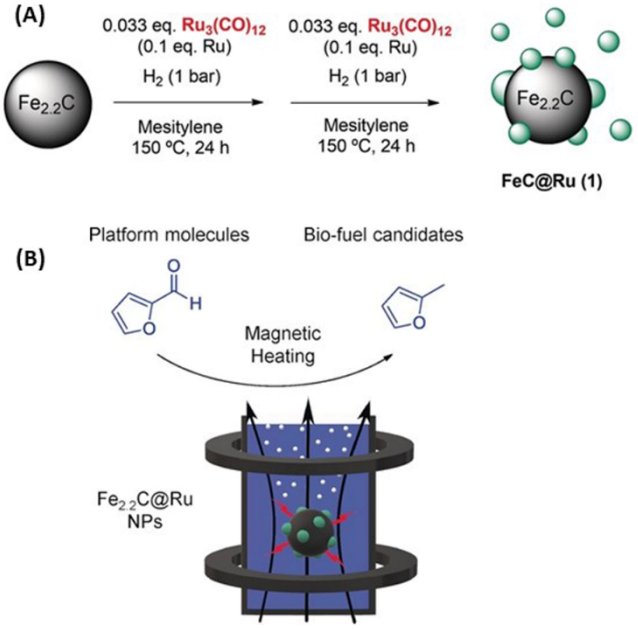

Figure 12: (A) Synthesis procedure of FeC@Ru NPs. (B) Representation of the magnetically induced catalysis of platform molecules to biofuel candidate molecules. Reprinted and adapted with permission from Ref.[63] Copyright 2019, Wiley-VCH.

Hybrid Co-based nanostructures, in the form of core/shell nano-objects, have been pursued with the aim of developing a new concept for detecting biomolecules. Briefly, the increase of the hydrodynamic radii of the magneto(Co)-plasmonic(Au) nanostructures formed by the capture of biomolecules at their surface can be accurately measured by exploiting the highly sensitive opto-magnetic detection of the relaxation dynamics of magnetically rotating magnetoplasmonic NPs.[66] The aim of this combined opto-magnetic sensing approach, is to reach detection limits down to the picomolar range and is, thus, technologically appealing for rapid point-of-care assays. Co@SnPtAu NRs of,

roughly, 5x70 nm were synthesized to test this new concept of *in-vitro* biosensing technology. Co NRs, were used as seeds to grow different metal layers. A buffer layer of $[Sn(NMe_2)_2]_2$ allows the growth of a quite homogeneous Pt layer completed by a deposition of Au (Figure 13).[67] After i) transferring the resulting NRs in water through the coating with an amphiphilic polymer and ii) functionalization with specified antibodies by linking the latter to the polymer backbone, Co@SnPtAu NRs were successfully tested in the detection of breast cancer biomarker sHER2 in serum and saliva samples.[68,69]

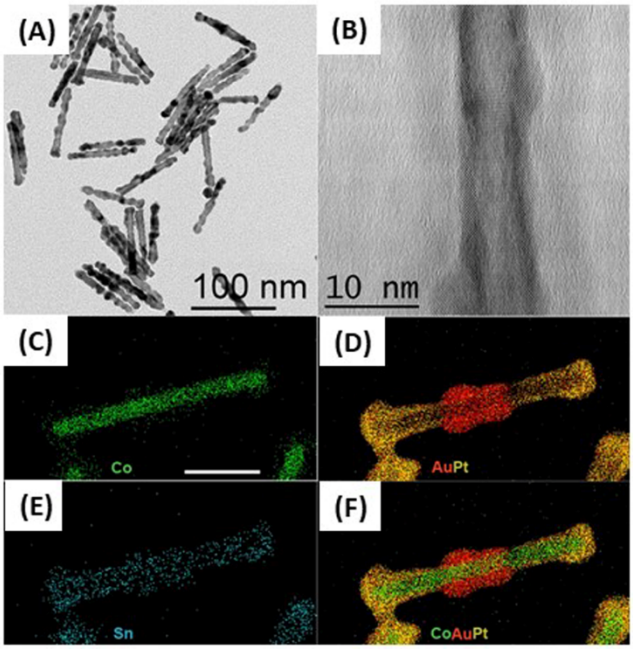

Figure 13: (A) TEM image of a Co@SnPtAu NR (scale bar: 100 nm). (B) HRTEM image on an isolated NR, revealing the polycrystalline nature of the shell (scale bar: 10 nm). (C-F) STEM- EDX maps showing the location of the elements on a fully covered NR (C: Co, D: Au and Pt, E: Sn, fF Co, Au and Pt). (Co: green, Sn: blue, Au: red Pt: yellow). Scale bar for all EDX maps is 20 nm. Reprinted with permission from Ref.[67] Copyright 2015, American Chemical Society.

3. CONCLUSIONS

The organometallic chemistry approach developed in Toulouse for over 20 years allows the preparation of small magnetic NPs of clean surface and of magnetic properties similar to those prepared in UHV.

This methodology, associated to the judicious choice of precursors and ligands and to the right reaction conditions in terms of temperature and pressure, can further allow the growth and the shaping of the NPs as well as the formation of bimetallic species which can be alloys, core-shell or NPs displaying a gradient of concentration. Growth of a new metal layer or of discrete NPs onto an existing NP is also possible leading to complex

nano-objects comprising for example a magnetic core, which can be heated by magnetic induction, and a catalytic surface or an external noble metal layer which can be useful for biodetection. Such magnetic NPs also find applications in the fields of micro-electronics or permanent magnets.

Overall, the precise design of chemical procedures derived from organometallic chemistry allows now the synthesis of complex nano-objects and nanomaterials, generally monodisperse, associated to a size, shape, composition and chemical order adapted to a desired property or application. Many of the nanostructures presented here cannot be produced by alternative methods, which renders the organometallic approach extremely useful, despite the fact that organometallic precursors have in general a higher cost than classical precursors and have to be handled with care. Since the NP syntheses employing these precursors can be scaled-up, this approach can allow the development of new materials of importance in the fields of catalysis and energy.

ACKNOWLEDGEMENTS:

The authors thank ERC AdG MONACAT-2015-694159 for support. M.E. acknowledges the grant RYC2018-024396-I funded by MCIN/AEI/ 10.13039/501100011033 and by "ESF Investing in your future''.

CONFLICT OF INTEREST:

The authors declare no conflict of interest.

KEYWORDS: Organometallic chemistry, nanoparticles, magnetic properties, catalysis

References

[1] S. Wang, J. Xu, W. Li, S. Sun, S. Gao, Y. Hou, *Chem. Rev.* **2022**, *122*, 5411–5475.

[2] G. A. Ozin, *Acc. Chem. Res.* **1977**, *10*, 21–26.

[3] S. C. Davis, K. J. Klabunde, *Chem. Rev.* **1982**, *82*, 153–208.

[4] G. N. Glavee, K. J. Klabunde, C. M. Sorensen, G. C. Hadjipanayis, *Langmuir* **1993**, *9*, 162–169.

[5] F. Fiévet, S. Ammar-Merah, R. Brayner, F. Chau, M. Giraud, F. Mammeri, J. Peron, J.-Y. Piquemal, L. Sicard, G. Viau, *Chem. Soc. Rev.* **2018**, *47*, 5187–5233.

[6] S. Sun, C. B. Murray, D. Weller, L. Folks, A. Moser, *Science* **2000**, *287*, 1989–1992.

[7] V. F. Puntes, D. Zanchet, C. K. Erdonmez, A. P. Alivisatos, *J. Am. Chem. Soc.* **2002**, *124*, 12874–12880.

[8] A. Duteil, R. Quéau, B. Chaudret, R. Mazel, C. Roucau, J. S. Bradley, *Chem. Mater.* **1993**, *5*, 341–347.

[9] J. Osuna, D. de Caro, C. Amiens, B. Chaudret, E. Snoeck, M. Respaud, J. M. Broto, A. Fert, *J. Phys. Chem.* **1996**, *100*, 14571–14574.

[10] M. Respaud, J. M. Broto, H. Rakoto, A. R. Fert, L. Thomas, B. Barbara, M. Verelst, E. Snoeck, P. Lecante, A. Mosset, J. Osuna, T. Ould Ely, C. Amiens, B. Chaudret, *Phys. Rev. B* **1998**, *57*, 2925–2935.

[11] M. Respaud, J. M. Broto, H. Rakoto, J. C. Ousset, J. Osuna, T. Ould Ely, C. Amiens, B. Chaudret, S. Askenazy, *Phys. Rev. B Condens. Matter.* **1998**, *246*, 532–536.

[12] T. Ould Ely, C. Amiens, B. Chaudret, E. Snoeck, M. Verelst, M. Respaud, J. M. Broto, *Chem. Mater.* **1999**, *11*, 526–529.

[13] F. Dassenoy, M.-J. Casanove, P. Lecante, M. Verelst, E. Snoeck, A. Mosset, T. Ould Ely, C. Amiens, B. Chaudret, *J. Chem. Phys.* **2000**, *112*, 8137-8145.

[14] D. Zitoun, C. Amiens, B. Chaudret, M. Respaud, M.-C. Fromen, P. Lecante, M.-J. Casanove, *New J. Phys.* **2002**, *4*, 77.1-77.11.

[15] N. Cordente, C. Amiens, B. Chaudret, M. Respaud, F. Senocq, M.-J. Casanove, *J. Appl. Phys.* **2003**, *94*, 6358–6365.

[16] Š. Pick, H. Dreyssé, *Surf. Sci.* **2000**, *460*, 153–161.

[17] O. Margeat, C. Amiens, B. Chaudret, P. Lecante, R. E. Benfield, *Chem. Mater.* **2005**, *17*, 107–111.

[18] N. Cordente, M. Respaud, F. Senocq, M.-J. Casanove, C. Amiens, B. Chaudret, *Nano Lett.* **2001**, *1*, 565–568.

[19] F. Dumestre, B. Chaudret, C. Amiens, M.-C. Fromen, M.-J. Casanove, P. Renaud, P. Zurcher, *Angew. Chem. Int. Ed.* **2002**, *41*, 4286–4289.

[20] F. Dumestre, B. Chaudret, C. Amiens, P. Renaud, P. Fejes, *Science* **2004**, *303*, 821–823.

[21] Z. A. Peng, X. Peng, *J. Am. Chem. Soc.* **2001**, *123*, 1389–1395.

[22] V. F. Puntes, K. M. Krishnan, P. A. Alivisatos, *Science* **2001**, *291*, 2115–2117.

[23] F. Dumestre, B. Chaudret, C. Amiens, M. Respaud, P. Fejes, P. Renaud, P. Zurcher, *Angew. Chem. Int. Ed.* **2003**, *42*, 5213–5216.

[24] F. Wetz, K. Soulantica, M. Respaud, A. Falqui, B. Chaudret, *Mater. Sci. Eng., C* **2007**, *27*, 1162–1166.

[25] N. Liakakos, B. Cormary, X. Li, P. Lecante, M. Respaud, L. Maron, A. Falqui, A. Genovese, L. Vendier, S. Koïnis, B. Chaudret, K. Soulantica, *J. Am. Chem. Soc.* **2012**, *134*, 17922–17931.

[26] B. Cormary, T. Li, N. Liakakos, L. Peres, P-F. Fazzini, T. Blon, M. Respaud, A. J. Kropf, B. Chaudret, J. T. Miller, E. A. Mader, K. Soulantica, *J. Am. Chem. Soc.* **2016**, *138*, 8422–8431.

[27] K. Soulantica, F. Wetz, J. Maynadié, A. Falqui, R. P. Tan, T. Blon, B. Chaudret, M. Respaud, *Appl. Phys. Lett.* **2009**, *95*, 152504.

[28] N. Liakakos, T. Blon, C. Achkar, V. Vilar, B. Cormary, R. P. Tan, O. Benamara, G. Chaboussant, F. Ott, B. Warot-Fonrose, E. Snoeck, B. Chaudret, K. Soulantica, M. Respaud, *Nano Lett.* **2014**, *14*, 3481–3486.

[29] N. Liakakos, C. Achkar, B. Cormary, J. Harmel, B. Warot-Fonrose, E. Snoeck, B. Chaudret, M. Respaud, K. Soulantica, T. Blon, *ACS Nano* **2015**, *9*, 9665–9677.

[30] J. Harmel, L. Peres, M. Estrader, A. Berliet, S. Maury, A. Fécant, B. Chaudret, P. Serp, K. Soulantica, *Angew. Chem. Int. Ed.* **2018**, *57*, 10579–10583.

[31] P. Kopčanský, N. Tomašovičová, M. Koneracká, V. Závišová, M. Timko, A. Džarová, A. Šprincová, N. Éber, K. Fodor-Csorba, T. Tóth-Katona, A. Vajda, J. Jadzyn, *Phys. Rev. E Stat. Nonlin. Soft Matter Phys.* **2008**, *78*, 011702.

[32] L. Zadoina, B. Lonetti, K. Soulantica, A.-F. Mingotaud, M. Respaud, B. Chaudret, M. Mauzac, *J. Mater. Chem.* **2009**, *19*, 8075–8078.

[33] O. Riou, L. Zadoina, B. Lonetti, K. Soulantica, A-F. Mingotaud, M. Respaud, B. Chaudret, M. Mauzac, *Polymers* **2012**, *4*, 448–462.

[34] J. Dugay, R. P. Tan, A. Meffre, T. Blon, L.-M. Lacroix, J. Carrey, P. F. Fazzini, S. Lachaize, B. Chaudret, M. Respaud, *Nano Lett.* **2011**, *11*, 5128–5134.

[35] E. Snoeck, C. Gatel, L.-M. Lacroix, T. Blon, S. Lachaize, J. Carrey, B. Chaudret, M. Respaud, *Nano Lett.* **2008**, *8*, 4293–4298.

[36] L.-M. Lacroix, S. Lachaize, A. Falqui, M. Respaud, B. Chaudret, *J. Am. Chem. Soc.* **2009**, *131*, 549–557.

[37] L.-M. Lacroix, S. Lachaize, F. Hue, C. Gatel, T. Blon, R. P. Tan, J. Carrey, B. Warot-Fonrose, B. Chaudret, *Nano Lett.* **2012**, *12*, 3245–3250.

[38] B. Mehdaoui, A. Meffre, L.-M. Lacroix, J. Carrey, S. Lachaize, M. Respaud, M. Gougeon, B. Chaudret, *J. Appl. Phys.* **2010**, *107*, 09A324.

[39] B. Mehdaoui, A. Meffre, L. M. Lacroix, J. Carrey, S. Lachaize, M. Goujeon, M. Respaud, B. Chaudret, *Bull. Cancer* **2010**, *97*, S57–S58.

[40] L. M. Lacroix, S. Lachaize, J. Carrey, M. Respaud, B. Chaudret, *Actual. Chim.* **2011**, *351*, 28–35.

[41] B. Mehdaoui, A. Meffre, J. Carrey, S. Lachaize, L.-M. Lacroix, M. Gougeon, B. Chaudret, M. Respaud, *Adv. Funct. Mater.* **2011**, *21*, 4573–4581.

[42] A. Bordet, L. M. Lacroix, P. F. Fazzini, J. Carrey, K. Soulantica, B. Chaudret, *Angew. Chem. Int. Ed.* **2016**, *55*, 15894–15898.

[43] A. Meffre, B. Mehdaoui, V. Kelsen, P. F. Fazzini, J. Carrey, S. Lachaize, M. Respaud, B. Chaudret, *Nano Lett.* **2012**, *12*, 4722–4728.

[44] J. M. Asensio, J. Marbaix, N. Mille, L.-M. Lacroix, K. Soulantica, P. F. Fazzini, J. Carrey, B. Chaudret, *Nanoscale* **2019**, *11*, 5402–5411.

[45] S. S. Kale, J. M. Asensio, M. Estrader, M. Werner, A. Bordet, D. Yi, J. Marbaix, P. F. Fazzini, K. Soulantica, B. Chaudret, *Catal. Sci. Technol.* **2019**, *9*, 2601–2607.

[46] T. Ould Ely, C. Pan, C. Amiens, B. Chaudret, F. Dassenoy, P. Lecante, M.-J. Casanove, A. Mosset, M. Respaud, J.-M. Broto, *J. Phys. Chem. B* **2000**, *104*, 695–702.

[47] D. Zitoun, C. Amiens, B. Chaudret, M.-C. Fromen, P. Lecante, M.-J. Casanove, M. Respaud, *J. Phys. Chem. B* **2003**, *107*, 6997–7005.

[48] D. Zitoun, M. Respaud, M.-C. Fromen, M.-J. Casanove, P. Lecante, C. Amiens, B. Chaudret, *Phys. Rev. Lett.* **2002**, *89*, 037203.

[49] D. Zitoun, M. Respaud, M.-C. Fromen, P. Lecante, M.-J. Casanove, C. Amiens, B. Chaudret, *J. Magn. Magn. Mater.* **2004**, *272*, 1536–1538.

[50] D. Ciuculescu, C. Amiens, M. Respaud, A. Falqui, P. Lecante, R. E. Benfield, L. Jiang, K. Fauth, B. Chaudret, *Chem. Mater.* **2007**, *19*, 4624–4626.

[51] A. Smekhova, D. Ciuculescu, P. Lecante, F. Wilhelm, C. Amiens, A. Rogalev, B. Chaudret, *IEEE Trans. Magn.* **2008**, *44*, 2776–2779.

[52] A. V. Trunova, J. Lindner, R. Meckenstock, M. Spasova, M. Farle, D. Ciuculescu, C. Amiens, B. Chaudret, M. Respaud, *J. Magn. Magn. Mater.* **2009**, *321*, 3502–3506.

[53] N. Atamena, D. Ciuculescu, G. Alcaraz, A. Smekhova, F. Wilhelm, A. Rogalev, B. Chaudret, P. Lecante, R. E. Benfield, C. Amiens, *Chem. Commun.* **2010**, *46*, 2453-2455.

[54] C. Desvaux, C. Amiens, P. Fejes, P. Renaud, M. Respaud, P. Lecante, E. Snoeck, B. Chaudret, *Nat. Mater.* **2005**, *4*, 750–753.

[55] C. Desvaux, F. Dumestre, C. Amiens, M. Respaud, P. Lecante, E. Snoeck, P. Fejes, P. Renaud, B. Chaudret, *J. Mater. Chem.* **2009**, *19*, 3268–3275.

[56] C. Garnero, M. Lepesant, C. Garcia-Marcelot, Y. Shin, C. Meny, P. Farger, B. Warot-Fonrose, R. Arenal, G. Viau, K. Soulantica, P. Fau, P. Poveda, L.-M. Lacroix, B. Chaudret, *Nano Lett.* **2019**, *19*, 1379–1386.

[57] A. Meffre, B. Mehdaoui, V. Connord, J. Carrey, P.-F. Fazzini, S. Lachaize, M. Respaud, B. Chaudret, *Nano Lett.* **2015**, *15*, 3241–3248.

[58] J. Marbaix, N. Mille, L.-M. Lacroix, J. M. Asensio, P.-F. Fazzini, K. Soulantica, J. Carrey, B. Chaudret, *ACS Appl. Nano Mater.* **2020**, *3*, 3767–3778.

[59] L. M. Martínez-Prieto, J. Marbaix, J. M. Asensio, C. Cerezo-Navarrete, P. F. Fazzini, K. Soulantica, B. Chaudret, A. Corma, *ACS Appl. Nano Mater.* **2020**, *3*, 7076–7087.

[60] O. Margeat, D. Ciuculescu, P. Lecante, M. Respaud, C. Amiens, B. Chaudret, *Small* **2007**, *3*, 451–458.

[61] D. De Masi, J. M. Asensio, P.-F. Fazzini, L.-M. Lacroix, B. Chaudret, *Angew. Chem. Int. Ed.* **2020**, *59*, 6187–6191.

[62] C. Niether, S. Faure, A. Bordet, J. Deseure, M. Chatenet, J. Carrey, B. Chaudret, A. Rouet, *Nat. Energy* **2018**, *3*, 476–483.

[63] J. M. Asensio, A. B. Miguel, P.-F. Fazzini, P. W. N. M. van Leeuwen, B. Chaudret, *Angew. Chem. Int. Ed.* **2019**, *58*, 11306–11310.

[64] Z. J. Díaz-Puerto, A. Raya-Barón, P. W. N. M. van Leeuwen, J. M. Asensio, B. Chaudret, *Nanoscale* **2021**, *13*, 12438–12442.

[65] I. Mustieles Marin, D. De Masi, L.-M. Lacroix, P.-F. Fazzini, P. W. N. M. van Leeuwen, J. M. Asensio, B. Chaudret, *Green Chem.* **2021**, *23*, 2025–2036.

[66] S. Schrittwieser, F. Ludwig, J. Dieckhoff, K. Soulantica, G. Viau, L.-M. Lacroix, S. M. Lentijo, R. Boubekri, J. Maynadié, A. Huetten, H. Brueckl, J. Schotter, *ACS Nano* **2012**, *6*, 791–801.

[67] S. Lentijo-Mozo, R. P. Tan, C. Garcia-Marcelot, T. Altantzis, P.-F. Fazzini, T. Hungria, B. Cormary, J. R. Gallagher, J. T. Miller, H. Martinez, S. Schrittwieser, J. Schotter, M. Respaud, S. Bals, G. Van Tendeloo, C. Gatel, K. Soulantica, *ACS Nano* **2015**, *9*, 2792–2804.

[68] S. Schrittwieser, B. Pelaz, W. J. Parak, S. Lentijo-Mozo, K. Soulantica, J. Dieckhoff, F. Ludwig, T. Altantzis, S. Bals, J. Schotter, *ACS Appl. Mater. Interfaces* **2016**, *8*, 8893–8899.

[69] S. Schrittwieser, B. Pelaz, W. J. Parak, S. Lentijo-Mozo, K. Soulantica, J. Dieckhoff, F. Ludwig, J. Schotter, *Sci. Rep.* **2017**, *7*, 4752.

TOC image

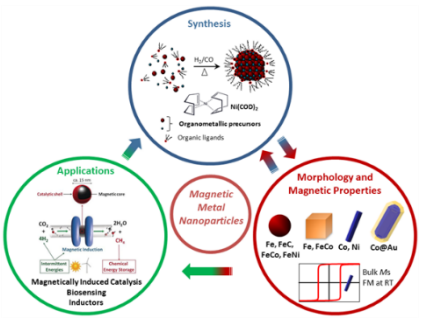

Text for Table of Contents: Magnetic metal nanoparticles (MMNPs) hold an important potential in a multitude of applications such as catalysis, biomedicine or environmental remediation. This Minireview highlights the advances over the last two decades of the organometallic synthesis of MMNPs. This synthesis approach has led to tailor-made sizes, shapes, compositions and magnetic properties of MMNPs leading to their application in magnetically induced catalysis and biosensing.